ISSN (Print) 1226-1750
ISSN (Online) 2233-6656
Journal of Magnetics 24(4), 568-576 (2019) https://doi.org/10.4283/JMAG.2019.24.4.568

Equivalent Circuit Model of Novel Solid Rotor Induction Motor with Toroidal Winding

Haichao Feng[1], Xu Cui[1], Jikai Si[2]*, Caixia Gao[1], and Chun Gan[3]

[1]*Henan Polytechnic University, No.2001 Century Avenue, Jiaozuo, China*
[2]*Zhengzhou University, No.100 Science Avenue, Zhengzhou, China*
[3]*Huazhong University of Science and Technology, Luoyu Road 1037, Wuhan, China*

(Received 5 May 2019, Received in final form 26 November 2019, Accepted 3 December 2019)

Solid rotor induction motor (SRIM) is widely used in many fields due to its sturdy construction, low maintenance costs, and soft mechanical characteristic. A novel SRIM with toroidal winding (N-TWSRIM) is proposed and its equivalent circuit model (ECM) is established herein. The structure of N-TWSRIM is introduced and its operating principle is analyzed according to the movement of armature magnetic field at different times. The main structural parameters of N-TWSRIM are given, an equivalent circuit model is established to analyze performance of motor, and the results of ECM and two-dimension finite element model (FEM) are compared. Finally, to validate the correctness of operating principle and equivalent circuit model, a prototype of N-TWSRIM has been built and experimented. It shows that the experimental results are consistent with the finite element and analytical results.

Keywords : equivalent circuit model, operating principle, solid-rotor induction motor, toroidal winding

1. Introduction

The novel solid rotor induction motor with toroidal winding (N-TWSRIM) consists of novel toroidal winding and solid rotor. It has the advantages of simple structure, flexible speed regulation and low maintenance cost [1]. Equivalent circuit model is an important method for motor design and performance analysis [2-4]. In order to quickly and intuitively analyze and calculate the performance of N-TWSRIM, it is crucial to establish an equivalent circuit model.

Due to the particularity of rotor structure, many scholars have done a lot of research for the analytical solution of the equivalent circuit model of SRIM. For the linear solution of the smooth solid rotor, the scholars use two-dimensional analytical method [5, 6], three-dimensional analytical method [7, 8] and other methods to calculate. Two-dimensional analytical method assumes that the rotor axial length is infinite, the core magnetic permeability is linear, no hysteresis and saturation phenomenon, and the rotor impedance angle is constant at 45°. Three-dimensional linear analytical calculation is mainly used to solve the end coefficient of the rotor impedance under the linear condition of the rotor. Solid rotor nonlinear analytical methods mainly include two-dimensional layering method [9], two-dimensional finite element [10-12] and so on. Two-dimensional layering method only considers the fundamental component of the magnetic field. The finite element method can consider the rotor saturation at the same time, but the physical meaning is not clear and the calculation amount is large.

In this paper, a novel solid rotor induction motor with toroidal winding (N-TWSRIM) is proposed. For this type of motor, the improved penetration depth method is used to calculate the motor parameters. Not only the rotor magnetic path nonlinearity but also the stator core nonlinearity can be considered. The paper is structured as follows. In Section 2, the structure and operating principle of N-TWSRIM is introduced. In Section 3, the main structure parameters are given, and equivalent circuit parameters are calculated by penetration depth method, the results are compared with the finite element method (FEM). In Section 4, a prototype is manufactured and tested, the correctness of equivalent circuit model, FEM and operating principle are verified. Finally, the conclusions of the paper are given in Section 5.

*Corresponding author: Tel: +8613523201034
Fax: +8613523201034, e-mail: sijikai527@126.com

2. Structure and Operating Principle of the N-TWSRIM

2.1. Motor Structure

Fig. 1 shows the stator winding wiring diagram and structure of the N-TWSRIM. The external surface of the stator core is welded with many pillars, which are connected with flanges. To increase the mechanical strength of the motor, the flanges are connected to an end cap. The N-TWSRIM relies on rotor bearings, flanges, and end caps to support its weight. Different from conventional motors, the winding of the N-TWSRIM are distributed in the same radial direction, and a coil is formed by the inner and outer winding surrounding the yoke of the stator. The current in the same side winding has the same direction. Each phase winding is composed of eight coils connected in a forward direction. The stator winding way of N-TWSRIM in this paper is different from the traditional motor, which can increase the pole pairs. This way not only can widen the speed regulation range of the motor, but also can long-term operation under heavy load or blocked conditions. In addition, the toroidal winding structure has better thermal diffusivity and lower maintenance costs than that of traditional winding. The stator winding of solid rotor induction motor (SRIM), traditional solid rotor induction motor with toroidal winding (T-TWSRIM) and N-TWSRIM are shown in Fig. 2. It can be seen from Fig. 2 that the stator winding of the N-

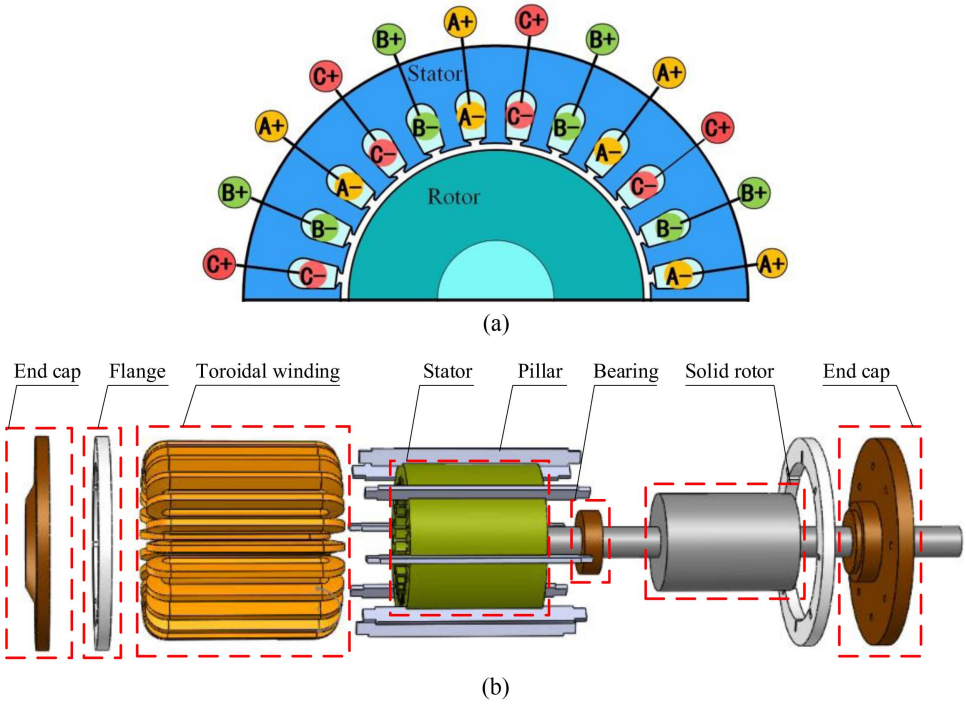

Fig. 1. (Color online) N-TWSRIM (a) Phase winding diagram, (b) N-TWSRIM structure.

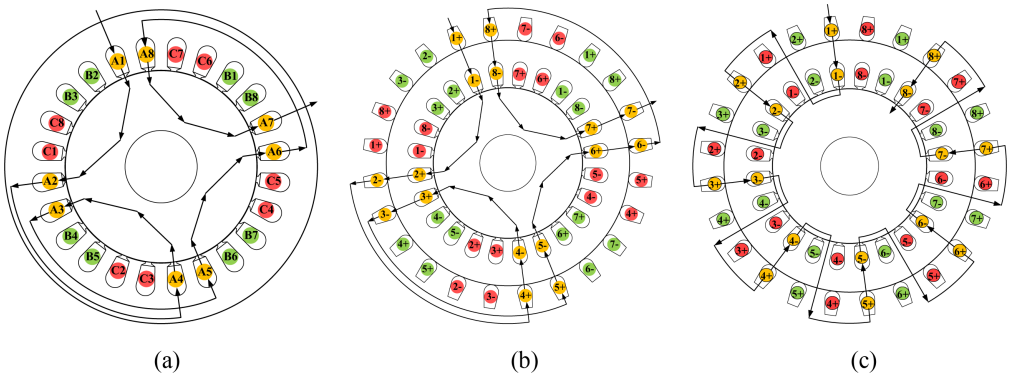

Fig. 2. (Color online) Stator winding structure. (a) SRIM, (b) T-TWSRIM, (c) N-TWSRIM.

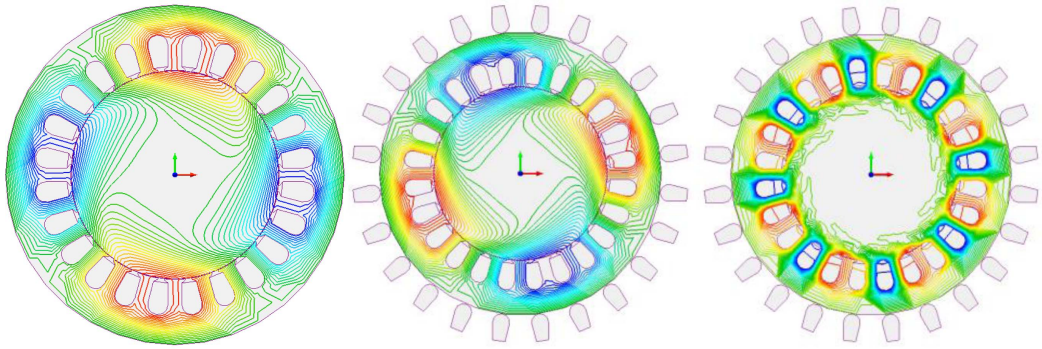

(a) (b) (c)

Fig. 3. (Color online) Stator winding magnetic field distribution. (a) SRIM, (b) T-TWSRIM, (c) N-TWSRIM.

TWSRIM is different from the one of the other two motors. It should be noted that not only are the stator winding of the proposed motor transferred from the stator tooth to the stator yoke, but also the incoming line ends of the stator winding is on the same side and have the same incoming direction.

Fig. 3 shows that the stator winding magnetic field distribution of three motor. We can see that the number of pole pairs of the proposed motor has increased, we can obtain a larger speed range.

2.2. Operating principle

The magnetic field in the motor changed due to the special winding connection of the N-TWSRIM. As a result, a new magnetic field is created. The operating principle is presented as follows.

Fig. 4 shows that the three-phase winding supply voltage waveform. Table 1 provides a list of the current directions for the three-phase winding at six time points ("+" for inflow and "–" for outflow).

Fig. 5 shows the changes in the armature magnetic field at different times. As we can see from Fig. 3, the comparison of the magnetic fields at point 1 and point 2

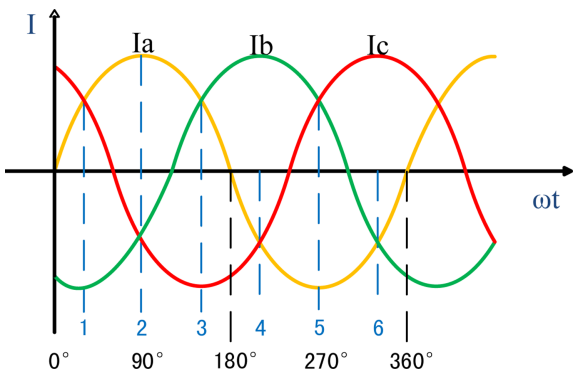

Fig. 4. (Color online) Three-phase winding supply voltage waveform.

Table 1. Three-phase winding current flow table at different points.

	1	2	3	4	5	6
A phase	+	+	+	–	–	–
B phase	–	–	+	+	+	–
C phase	+	–	–	–	+	+

shows that the N pole of the armature magnetic field has no movement, but the S pole moves 120 electrical angles in the counter-clockwise direction. Compared with the situations at Point 2 and point 3, The S pole of the armature magnetic field has no moving position, and the N pole moves 120 electrical angles in the counter-clockwise direction. Compared with the situations at Point 3 and point 4, the N pole of the armature magnetic field has

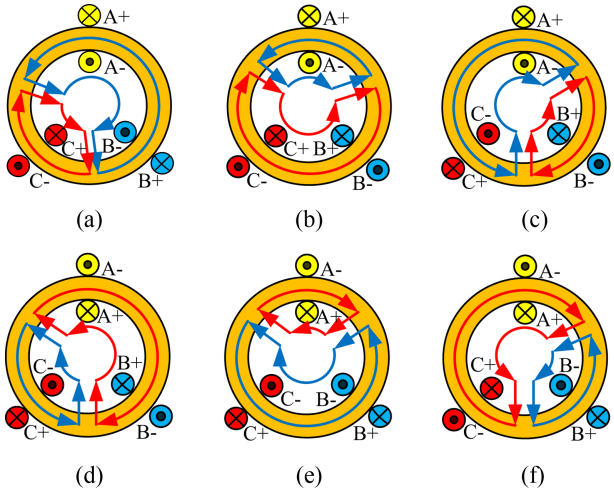

Fig. 5. (Color online) Armature magnetic fields of motor at different points (a) Armature magnetic field at point 1; (b) armature magnetic field at point 2; (c) armature magnetic field at point 3; (d) armature magnetic field at point 4; (e) armature magnetic field at point 5; (f) armature magnetic field at point 6.

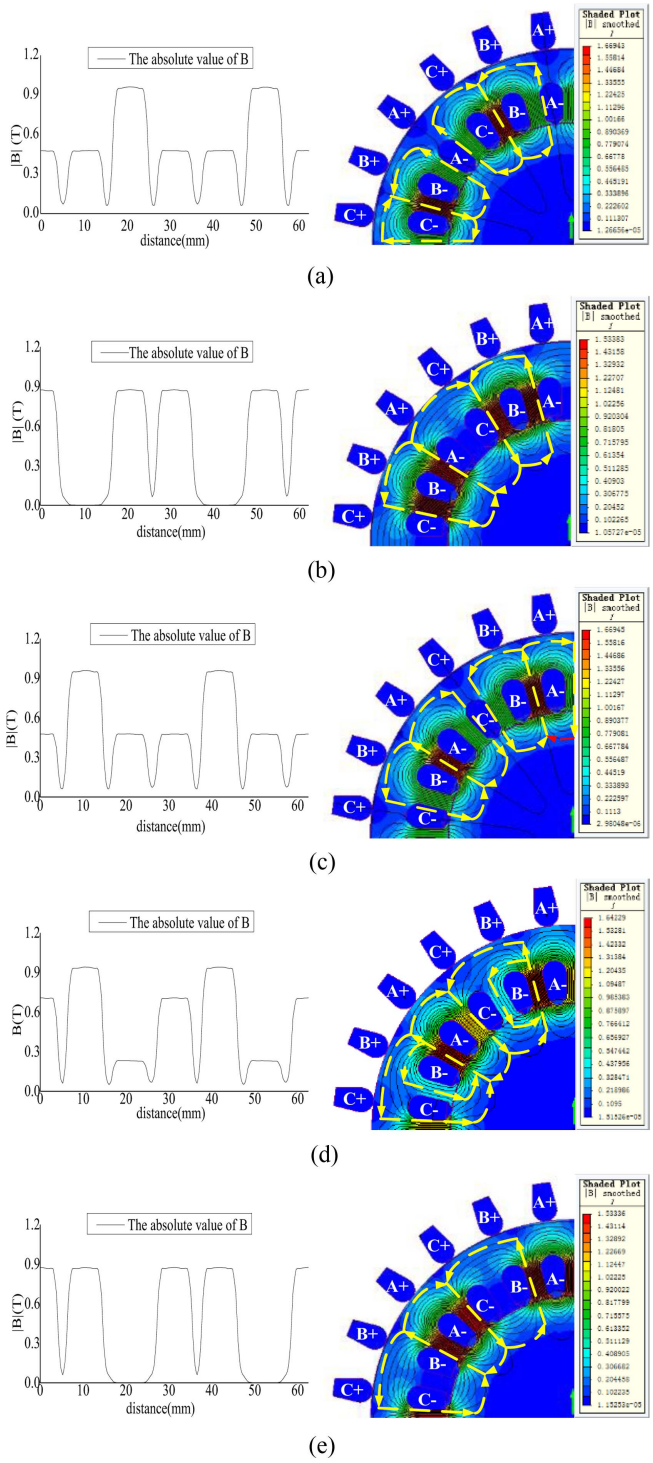

Fig. 6. (Color online) air-gap flux density and magnetic field distribution at different times (a) 0° times; (b) 30° times; (c) 60° times; (d) 75° times; (e) 90° times.

no moving position, and the S pole moves 120 electrical angles in the counter-clockwise direction. Compared with the situations at Point 4 and point 5, the S pole of the armature magnetic field has no moving position, and the N pole moves 120 electrical angles in the counter-clockwise direction. Compared with the situations at Point 5 and point 6, the N pole of the armature magnetic field has no moving position, and the S pole moves 120 electrical angles in the counter-clockwise direction. It can be concluded that the armature magnetic field of three-slot unit motor forms a pair of poles and changes periodically.

The special winding form makes the magnetic field of the motor change, and the pole number is doubled. To analyze the change of N-TWSRIM magnetic field, take 1/4 N-TWSRIM as an example, Fig. 6 shows air-gap flux density and the magnetic field distribution at different times. Comparing Fig. 6a to Fig. 6e, it can be concluded that when any phase voltage amplitude of the three-phase voltage crosses zero, the armature magnetic field distribution area is equal, as shown in Fig. 6a, Fig. 6c; When the amplitude of any phase voltage reaches the maximum value, the armature magnetic field is not equal, as shown in Fig. 6b and Fig. 6e. As can be seen from Fig. 6d, the armature magnetic field distribution is a transition phase, so the magnetic field not obvious. The air gap magnetic density curve also verifies this phenomenon.

2.3. Major parameter

Considering the particularity of the motor design, the preliminary design of the motor is based on the design method of the asynchronous motor. When the preliminary design is carried out, the stator core uses the Y series asynchronous motor Y90L-4, the stator core material is

Table 2. Main parameters of N-TWSRIM.

Parameters	Values
Rated voltage U_N (V)	220
Rated frequency f (Hz)	50
Stator outer diameter D_o (mm)	130
Stator inner diameter D_i (mm)	80
Rotor outer diameter D_r (mm)	79.3
Length of stator core L_{ef} (mm)	110
Length of rotor L_{ef} (mm)	110
Air gap δ (mm)	0.35
Stator pole number p	8
Number of stator slots Z_{stator}	24

Table 3. Materials information of N-TWSRIM.

Item	Material	Conductivity	Relative permeability
Stator	silicon steel plate M470-50A	3.2 MS/m	8000
Winding	copper	57.7 MS/m	1
Rotor	Steel Q235A	5 MS/m	400

silicon steel plate V200-50B, the stator winding connection type is Y, the rotor is smooth solid rotor, and rotor core material is steel E235. The main parameters of N-TWSRIM are shown in Table 2, the information of materials is shown in Table 3.

3. Equivalent Circuit Model of the N-TWSRIM

The smooth solid rotor motor is the most basic structural model in the solid rotor motor. The calculation of the equivalent circuit parameters is the basis for studying other types of solid rotor motors. The equivalent circuit is the main method to study the electromagnetic theory, working characteristics and design calculation of solid rotor induction motor.

The T type equivalent circuit model [5] for N-TWSRIM is shown in Fig. 7. U_1 is the input phase voltage, I_1 is the stator current, R_1 is the stator winding resistance, X_1 is the stator leakage reactance, E is the EMF, X_{mg} is the excitation reactance, I_r is the rotor current. The rotor impedance Z_r contains the rotor resistance R_r and rotor leakage reactance X_r. The equivalent circuit characterizes the energy transfer relationship between stator and rotor.

One approximate way to obtain the equivalent resistance

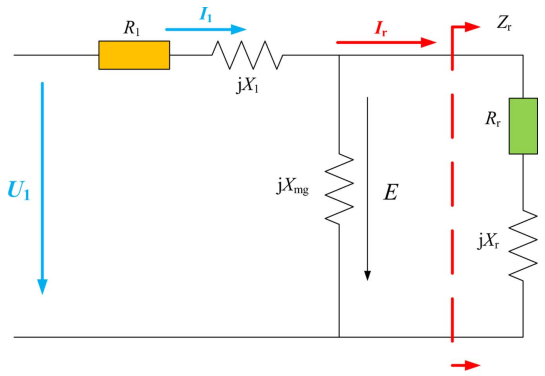

Fig. 7. (Color online) Equivalent circuit model.

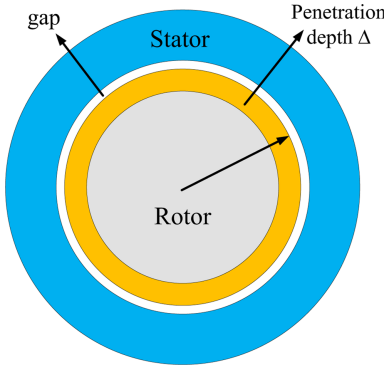

Fig. 8. (Color online) Schematic diagram of penetration depth.

of solid rotor depends on the eddy currents' penetration depth. As shown in Fig. 8, eddy currents in the rotor are viewed as evenly distributed currents in the shaded area within the penetration depth. According to the definition of penetration depth, the following assumptions are made.

1. It is considered that the rotor eddy flows only in a thin plate of width πD_r, thickness Δ, and length L_{ef}.
2. The eddy current density along the thickness Δ is constant and uniform distributed.
3. The eddy current flows only in the axial direction and closes at infinity. There is no tangential and radial eddy current component within the length of L_{ef}.
4. The stator core is not saturated, its magnetic permeability is infinite, and the conductivity is 0.

Equivalent circuit parameters are calculated by penetration depth method [13]. The rotor equivalent resistance R_r converted to the stator side can be directly obtained from the penetration depth and Ohm's law.

$$R_r = \frac{m_1(N_{\phi 1}K_{dp1})^2}{s}\rho_2\frac{L_{ef}}{\pi D_r\Delta}K_rK_eK_1 \tag{1}$$

$$X_r = \frac{m_1(N_{\phi 1}K_{dp1})^2}{s}\rho_2\frac{L_{ef}}{\pi D_r\Delta}K_XK_eK_1 \tag{2}$$

Where, m_1 is the number of phases, $N_{\phi 1}$ is the number of series turns per phase, K_{dp1} is the winding factor, s is the slip, ρ_2 is the rotor resistivity, L_{ef} is the length of rotor, K_r is the resistance correction factor, K_e is the end effect factor, K_1 is the correction factor, K_X is the reactance correction factor.

The eddy currents' penetration depth Δ is

$$\Delta = \sqrt{\frac{2}{\omega\mu_r\mu_o\sigma}} = \sqrt{\frac{2\rho_2}{s\omega_1\mu_r\mu_o}} = \sqrt{\frac{2\rho_2}{\omega_1\mu_o}}\sqrt{\frac{1}{s\mu_r}} \tag{3}$$

Where, ω_1 is the source angular frequency, μ_0 is the permeability of vacuum, μ_r is the relative permeability.

K_e and K_1 can be expressed as

$$K_e = \left(1+\frac{\tau}{L_{ef}}\right)\frac{a^2\delta+\dfrac{1}{\Delta\mu_r}}{\gamma^2\delta+\dfrac{1}{\Delta\mu_r}} \tag{4}$$

Where, τ is the pole pitch, $a=\pi/\tau$, $\gamma = a\times\sqrt{1+(\tau/L_{ef})^2}$.

$$K_1 = \frac{D_r^2}{\left(D_r-\dfrac{2}{3}\Delta\right)^2} \tag{5}$$

Referring to the motor design th eory[14], when the stator permeability is infinite, the main excitation reactance.

$$X_m = \frac{4f\mu_0 m(N_{\phi 1}K_{dp1})^2\tau L_{ef}}{\pi\delta p} \tag{6}$$

The main excitation reactance X'_m considering the stator saturation is required to be divided by the saturation coefficient K_s on the basis of equation (6).

$$X'_m = \frac{4f\mu_0 m(N_{\phi 1}K_{dp1})^2 \tau L_{ef}}{\pi \delta p K_s} \tag{7}$$

In this paper, the difference between the structure of the proposed motor and the traditional motor structure mainly exists in the wiring of the stator winding. Therefore, the important point of this paper is the parameter calculation of stator winding. The stator side resistance and reactance are calculated by equation (1-3).

$$R_1 = K'_F \rho_\omega \frac{2N_1 l_s}{a_1 A_{01}} \tag{8}$$

$$X_1 = 4f\mu_0 \frac{m}{\pi}\frac{(NK_{dp1})^2}{p} l_s \frac{\tau}{\delta} \tag{9}$$

$$l_s = 2(l_{ef} + 2d_1 + K_1 \tau_y) \tag{10}$$

Where, R_1 is the stator resistance, X_1 is the stator reactance, number of parallel branches, l_s is the stator length of winding, ρ_ω is the conductor resistivity, A_{01} is winding cross-sectional area, K'_F, K_1 are the winding coefficient and the end coefficient, respectively.

According to the impedance value calculated by the above formula, some motor performance can be calculated.

$$I_1 = \frac{E_2}{Z_m} + \frac{E_2}{Z_r} \tag{11}$$

$$T_{em} = \frac{P_{em}}{\omega_1} = \frac{m_1 E_2 I_r}{2\pi f_1} \tag{12}$$

In the case where the stator winding phase voltage is 220 V and the voltage frequency is 50 Hz, the rotor equivalent parameters of the solid rotor motor of the toroidal winding are calculated. The results are shown in Table 4.

The process of solving magnetic fields while considering saturation is listed below, and Fig. 9 shows the computational program diagram of N-TWSRIM.

Table 4. Rotor impendence parameter calculation under different load condition.

Slip	value
0.3	557.75 ∠ 35°
0.4	483.03 ∠ 35°
0.5	432.03 ∠ 35°
0.6	394.39 ∠ 35°
0.7	365.13 ∠ 35°
0.8	341.55 ∠ 35°
0.9	322.02 ∠ 35°

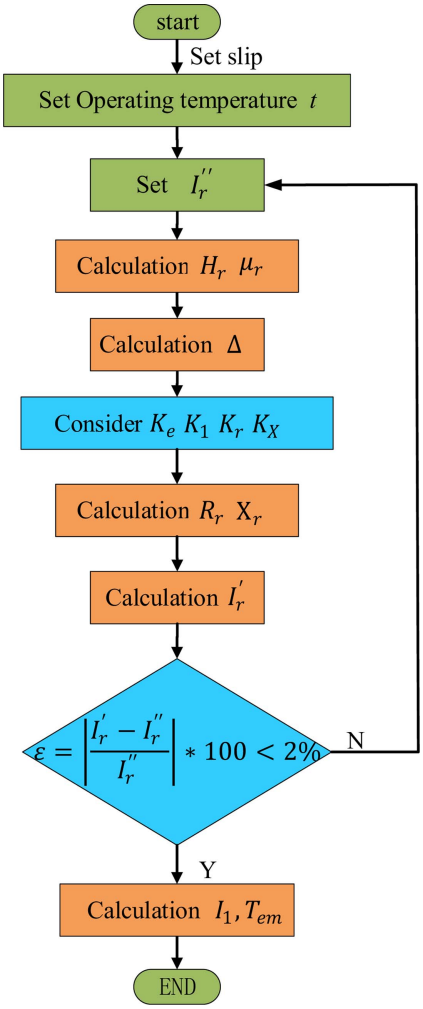

Fig. 9. (Color online) Computational program diagram of N-TWSRIM.

According to the data given in Table 2, the finite element model is established, and the two-dimensional time harmonic electromagnetic field is used to solve model. The slip range is set from 0.3 to 0.9.

We can calculate some characteristics of the motor, such as stator phase current, electromagnetic torque, and rotor copper loss from the equivalent circuit parameters and characteristic calculation formula. After the stator phase current is decomposed by Fourier series, the current amplitude curve at different slip rates is defined, as shown in Fig. 10(a). The electromagnetic torque curves at different slip rates are shown in Fig. 10(b). The error between ECM and FEM is shown in Table 5.

As shown in Fig. 10, the calculation result of the equivalent circuit has good consistency with the calculation result of the finite element method, and the maximum error does not exceed 15 %. These findings prove the

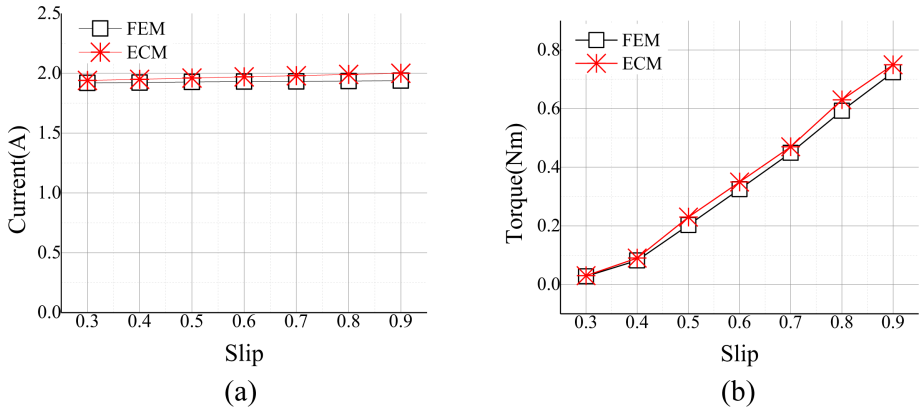

Fig. 10. (Color online) Comparative Results of ECM and FEM. (a) Stator phase current at different slip rates, (b) Electromagnetic torque under different slip rates.

Table 5. Stator current comparison result under different slip.

Slip	Stator current			Output torque		
	FEM	ECM	Error	FEM	ECM	Error
0.3	1.920	1.94	1.03 %	0.028	0.03	6.67 %
0.4	1.922	1.95	1.43 %	0.082	0.10	8.89 %
0.5	1.928	1.96	1.63 %	0.203	0.23	11.7 %
0.6	1.930	1.97	2.03 %	0.325	0.35	7.14 %
0.7	1.932	1.98	2.42 %	0.449	0.47	4.47 %
0.8	1.934	1.99	2.81 %	0.593	0.63	5.87 %
0.9	1.939	2.01	3.53 %	0.724	0.75	3.47 %

correctness of the equivalent circuit.

4. Result Verification

To verify the accuracy of the results presented above, a novel SRIM with toroidal winding is designed and manufactured. The prototype processing is shown in Fig. 11, and the motor experimental platform is shown in Fig. 12.

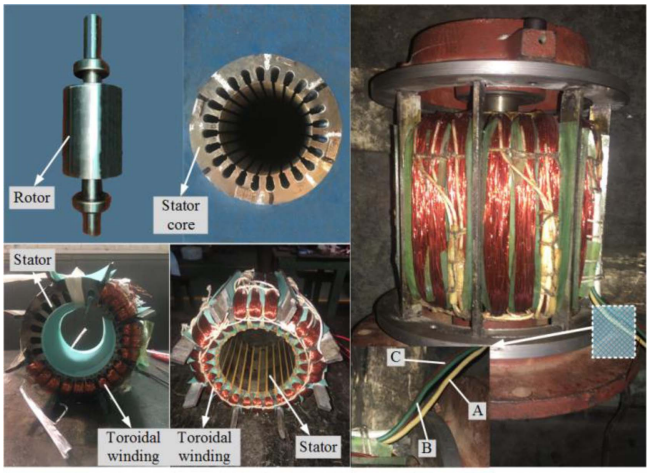

Fig. 11. (Color online) Prototype processing.

Fig. 12. (Color online) Prototype testing platform.

In the Fig. 12, The speed and torque of the prototype are measured by the torque-speed sensor. The load torque is provided by the eddy current brake, and eddy current brake and measuring instrument are connected by the coupling. The power supply of the prototype is provided by ABB inverter.

The prototype experiment is carried out under the condition of the stator winding voltage, RMS voltage of

Table 6. Stator current comparison result under different slip.

Slip	ECM	FEM	Measured
0.3	1.94A	1.920A	2.016A
0.4	1.95A	1.922A	2.019A
0.5	1.96A	1.928A	2.024A
0.6	1.97A	1.930A	2.032A
0.7	1.98A	1.932A	2.042A
0.8	1.99A	1.934A	2.056A
0.9	2.01A	1.939A	2.070A

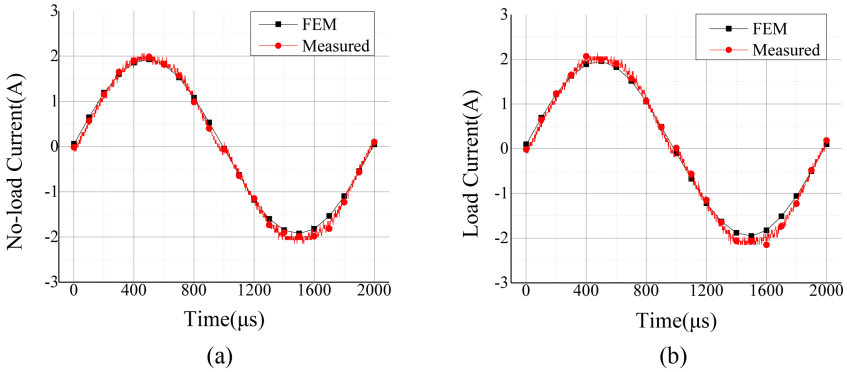

Fig. 13. (Color online) Simulation and experimental stator current.

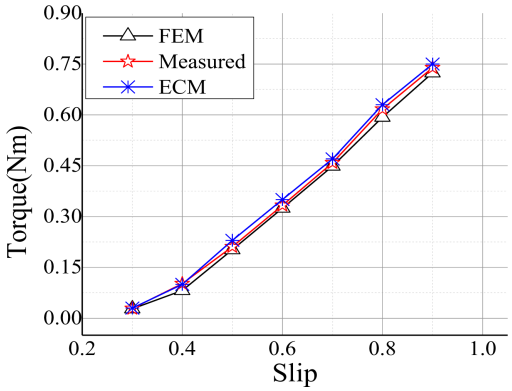

Fig. 14. (Color online) Torque-slip curve comparison.

220 V, and voltage frequency of 50 Hz. The experimental results are compared with the finite element results. The rotor parameters on the experimental prototype cannot be separately measured, so the output torque and stator current at different slips are selected as comparison indicators. Fig. 13 shows the stator current curves of the simulation and experiment at no load and load, respectively. Table 6 gives the analytical, finite element and experimental current values for different slip.

As shown in Fig. 13, the stator current waveforms of the simulation and experiment have good consistency, and the current amplitude has only a small increase under no-load and full-load conditions. Fig. 14 show the curves of torque-slip curve under equivalent circuit model, simulation, and experiment. The differences between ECM results and measured results is shown in Table 7. Error 1 is the error between ECM and FEM, Error 2 is the error between ECM and Measured.

As shown in Fig. 14, the equivalent circuit model and simulation results are agreed with the experimental results, and output torque rises as the slip rate increases. Thus, the correctness of the equivalent circuit model and simulation results is verified.

Table 7. Out torque comparison result.

Slip	ECM (Nm)	FEM (Nm)	Measured (Nm)	Error1	Error2
0.3	0.03	0.028	0.029	3.44 %	3.45 %
0.4	0.1	0.082	0.089	1.96 %	8.89 %
0.5	0.23	0.203	0.211	9.0 %	3.79 %
0.6	0.35	0.325	0.333	5.10 %	2.40 %
0.7	0.47	0.449	0.459	2.39 %	2.18 %
0.8	0.63	0.593	0.617	2.11 %	3.89 %
0.9	0.75	0.724	0.739	1.48 %	2.03 %

5. Conclusions

In this paper, a novel SRIM with toroidal winding is presented and studied. It can combine the advantages of a solid rotor and a toroidal winding, not only for harsh conditions, but also when a fault (short circuit or open circuit)) occurred in either coil, the toroidal configuration can solve this problem by replacing a single coil. So, the reliability of motor under various faulty conditions was enhanced. The operating principle of the motor is analyzed by the change of the magnetic field at different electrical angles. The equivalent circuit model is given and its parameters are calculated by the penetration depth method. The electromagnetic performances including torque and stator current under different slip are predicted, and the results are verified by 2D-FEA. At the same time, the prototype of N-TWSRIM is fabricated and tested. The results show that the experimental results are consistent with the two-dimensional finite element results and analytical results. It can be found that the designed N-TWSRIM is feasible and the equivalent circuit model of N-TWSRIM is effective.

Acknowledgement

This work was supported by National Natural Science

Foundation of China under grant 51777060 and 51277054, the Key Science and Technology National Program of Henan Province No. 192102210230. The prototype was produced by Yokogawa Robot (Shenzhen) Co., Ltd. Thanks to Shu-hua Wang for technical support. The motor control system was provided by Zhengzhou Runhua Industrial Automation Equipment Co., Ltd., thanks to Ying-sheng Li for providing technical support.

References

[1] Cui Xu, Si Jikai, and Feng Haichao, Trans. China Electrotech. Soc. **34**, 1850 (2019).
[2] Huang Ziguo, Wang Shanming, and Ni Shouhui, Proceedings of CSEE **36**, 2505 (2016).
[3] Ling Zaiwei, Zhou Libing, Zhang Yi, and Li Langru, Trans. China Electrotech. Soc. **33**, 3518 (2018).
[4] Chang Zhengfeng, Nanjing University of Aeronautics and Astronautics, China (2007).
[5] Feng Erjian, Ferromagnetic solid rotor asynchronous motor theory and calculation, Feng Erjian, China (1980) pp 15-80.
[6] Gang Lv, Shaoqiang Yan, Dihui Zeng, and Tong Zhou, IET Electric Power Applications **13**, 31 (2019).
[7] Tang Xiaogao, Solid rotor asynchronous motor and its application, Tang Xiaogao, C China (1991) pp 1-40.
[8] Yee, H., Effects of finite length in solid-rotor induction machines[C]//Proceedings of the Institution of Electrical Engineers **8**, 1025 (1971).
[9] Greig, J. and Freeman, E. M., Proceedings of the Institution of Electrical Engineers **11**, 1681 (1967).
[10] Wu Xinzhen and Wang Xiangheng, Proceedings of the CSEE **18**, 23 (2007).
[11] Liu Changhong and Yao Ruoping, Journal of Shanghai Jiaotong University **9**, 1372 (2003).
[12] Sun Yanye and Yu Lie, Proceedings of CSEE **2**, 116 (2002).
[13] Fu Fengli and Tang Xiaogao, Handbook of asynchronous motor design, Fu Fengli, China (2002) pp 578-583.
[14] Chen Shikun, Electric machine design, Chen Shikun, China (1990) pp 50-65.